Chiral extrapolation of nucleon magnetic moments at next-to-leading-order

P. Wang,[1,2] D. B. Leinweber,[3] A. W. Thomas,[3,4] and R. D. Young[3,4]

[1]*Institute of High Energy Physics, CAS, P.O. Box 918(4), Beijing 100049, China*
[2]*Theoretical Physics Center for Science Facilities, CAS, Beijing 100049, China*
[3]*Special Research Center for the Subatomic Structure of Matter (CSSM), School of Chemistry & Physics, University of Adelaide, South Australia 5005, Australia*
[4]*ARC Centre of Excellence in Particle Physics at the Terascale, School of Chemistry & Physics, University of Adelaide, South Australia 5005, Australia*

(Received 19 October 2012; published 26 November 2012)

Nucleon magnetic moments display a rich nonanalytic dependence on the quark mass in both quenched and full QCD. They provide a forum for a detailed examination of the connection between quenched and full QCD made possible through the formalism of finite-range regularized chiral effective field theory. By defining meson-cloud and core contributions through the careful selection of a regularization scale, one can correct the meson cloud of quenched QCD to make full QCD predictions. Whereas past success is based on unquenching the leading-order loop contributions, here we extend and test the formalism including next-to-leading-order loop contributions. We discuss the subtleties associated with working at next-to-leading order and illustrate the role of higher-order corrections.

DOI: 10.1103/PhysRevD.86.094038 PACS numbers: 21.10.Ky, 12.39.Fe, 14.20.Dh

I. INTRODUCTION

The study of the properties of hadrons continues to attract significant interest in the process of revealing and understanding the essential mechanisms of QCD, the fundamental theory of the strong interactions. The nonperturbative properties of QCD and the difficulty of numerically simulating the theory at the light quark masses of nature has provided a rich history of phenomenological models at both the quark and hadronic levels and an intense study of the quark-mass dependence of hadronic observables in effective field theory (EFT).

Based on the observation that *all* hadron properties show a slow, smooth variation with quark mass for pion masses above $m_\pi \sim 0.4$ GeV, one can conclude that the nonanalytic contributions from pion loops are suppressed there [1]. An alternative regularization method, namely, finite-range regularization (FRR), resums the chiral expansion in a manner that suppresses loop contributions at large pion masses. Inspired by quark models [2–4] that account for the finite size of the nucleon as the source of the pion cloud, FRR EFT has been used to describe lattice data over a wide range of pion masses.

FRR EFT was first applied in the extrapolation of the nucleon mass and magnetic moments [5–7]. The remarkably improved convergence properties of the FRR expansion mean that lattice data at large pion masses can be described very well, and the nucleon mass obtained at the physical pion mass compared favorably with the experimental value. Later, the FRR method was applied to extrapolate the vector meson mass, magnetic moments, magnetic form factors, strange form factors, charge radii, first moments of generalized parton distributions, etc. [8–16]. The results are reasonable and reflect the manner in which FRR EFT characterizes the essential features of QCD at the hadronic level.

The prevalence of the quenched approximation in the history of lattice QCD simulations provided an opportunity to explore the possible connection between quenched and full QCD data. Indeed quenched chiral perturbation theory was developed [17–21] to understand how the nonanalytic structure of quenched QCD differed from that of full QCD. It was the advent of FRR EFT that made it possible to define a pion-cloud contribution to hadronic observables and then proceed to correct the quenched cloud to that of full QCD [22].

The meson loop contributions are calculated in both quenched and full QCD in terms of the axial coupling constants. One then fits the quenched FRR EFT to lattice QCD to learn the low-energy coefficients. This is done by fitting the coefficients of the residual series of terms analytic in the quark mass. The value of the nucleon axial charge, g_A, from a quenched lattice simulation with domain wall fermions is about 1.21 [23]. This value is almost the same as the full lattice QCD result [24–26]. The pion decay constant in quenched lattice QCD is about 89 MeV [27], which is only 5% smaller than the physical value. Therefore, with the assumption that the SU(3) axial coupling constants, F, D, and $\mathcal{C}$ as well as pion decay constant f_π, do not differ significantly between quenched and full QCD, one can replace the quenched meson cloud contribution of FRR EFT with the full QCD cloud contribution. Because the loop contribution in the quenched case at finite volume is small, this replacement will not cause a significant difference. We note that in dimensional regularization, for example, the low-energy coefficients are composed of both residual series and loop contributions with no recourse to separating the origin of terms

contributing to the total renormalized coefficient. On the contrary, in FRR the low energy coefficients of the residual analytic expansion provide the core contribution which is considered invariant in moving from quenched QCD to full QCD.

The dependence of the nucleon magnetic moments on quark mass has been studied by various chiral perturbation theory groups and lattice collaborations [28–41]. Quenched and partially quenched FRR chiral EFT has been used to study baryon electromagnetic phenomena including charge radii, strange magnetic moments, and strange form factors [12–15]. In the previous calculations, only the leading-order diagrams were included and unquenched. For example, power counting with $M_\Delta = M_N$ for the magnetic form factor, only the leading nonanalytic terms proportional to $\log(m_\pi)$ and m_π were included. In this paper, we will include the next-to-leading-order (NLO) contributions.

The paper is organized in the following way. In Sec. II, we briefly introduce the relevant chiral Lagrangian. In Sec. III, we study the nucleon magnetic moments using chiral perturbation theory with FRR at NLO. Numerical results and discussions are presented in Sec. IV. Finally, Sec. V provides a summary.

II. CHIRAL LAGRANGIAN

There are many papers that deal with heavy baryon chiral perturbation theory—for details, see, for example, Refs. [42–44]. For completeness, we briefly introduce the formalism in this section. In heavy-baryon chiral perturbation theory, the lowest chiral Lagrangian for the baryon-meson interaction that will be used in the calculation of the nucleon magnetic moments, including the octet and decuplet baryons, is expressed as

$$\begin{aligned}\mathcal{L}_v &= i\mathrm{Tr}\bar{B}_v(v\cdot\mathcal{D})B_v + 2D\mathrm{Tr}\bar{B}_v S_v^\mu\{A_\mu, B_v\}\\ &\quad + 2F\mathrm{Tr}\bar{B}_v S_v^\mu[A_\mu, B_v] - i\bar{T}_v^\mu(v\cdot\mathcal{D})T_{v\mu}\\ &\quad + \mathcal{C}(\bar{T}_v^\mu A_\mu B_v + \bar{B}_v A_\mu T_v^\mu),\end{aligned} \tag{1}$$

where S_μ is the covariant spin-operator defined as

$$S_v^\mu = \frac{i}{2}\gamma^5\sigma^{\mu\nu}v_\nu. \tag{2}$$

Here, v^ν is the nucleon four velocity (in the rest frame, we have $v^\nu = (1, 0)$). D, F, and $\mathcal{C}$ are the axial coupling constants. The chiral covariant derivative D_μ is written as $D_\mu B_v = \partial_\mu B_v + [V_\mu, B_v]$. The pseudoscalar meson octet couples to the baryon field through the vector and axial vector combinations

$$\begin{aligned}V_\mu &= \frac{1}{2}(\zeta\partial_\mu\zeta^\dagger + \zeta^\dagger\partial_\mu\zeta),\\ A_\mu &= \frac{1}{2}(\zeta\partial_\mu\zeta^\dagger - \zeta^\dagger\partial_\mu\zeta),\end{aligned} \tag{3}$$

where

$$\zeta = e^{i\phi/f_\pi}, \qquad f_\pi = 93\ \mathrm{MeV}. \tag{4}$$

The matrix of pseudoscalar fields ϕ is expressed as

$$\phi = \frac{1}{\sqrt{2}}\begin{pmatrix} \frac{1}{\sqrt{2}}\pi^0 + \frac{1}{\sqrt{6}}\eta & \pi^+ & K^+ \\ \pi^- & -\frac{1}{\sqrt{2}}\pi^0 + \frac{1}{\sqrt{6}}\eta & K^0 \\ K^- & \bar{K}^0 & -\frac{2}{\sqrt{6}}\eta \end{pmatrix}. \tag{5}$$

B_v and T_v^μ are the velocity dependent new fields that are related to the original baryon octet and decuplet fields B and T^μ by

$$B_v(x) = e^{im_N\not{v}_\mu x^\mu}B(x), \tag{6}$$

$$T_v^\mu(x) = e^{im_N\not{v}_\mu x^\mu}T^\mu(x). \tag{7}$$

In the chiral $SU(3)$ limit, the octet baryons will have the same mass m_B. In our calculation, we use the physical masses for the baryon octets and decuplets. The explicit form of the baryon octet is written as

$$B = \begin{pmatrix} \frac{1}{\sqrt{2}}\Sigma^0 + \frac{1}{\sqrt{6}}\Lambda & \Sigma^+ & p \\ \Sigma^- & -\frac{1}{\sqrt{2}}\Sigma^0 + \frac{1}{\sqrt{6}}\Lambda & n \\ \Xi^- & \Xi^0 & -\frac{2}{\sqrt{6}}\Lambda \end{pmatrix}. \tag{8}$$

For the baryon decuplet, the symmetric tensor carries three indices and is defined as

$$\begin{aligned}&T_{111} = \Delta^{++}, \quad T_{112} = \frac{1}{\sqrt{3}}\Delta^+, \quad T_{122} = \frac{1}{\sqrt{3}}\Delta^0, \quad T_{222} = \Delta^-,\\ &T_{113} = \frac{1}{\sqrt{3}}\Sigma^{*,+}, \quad T_{123} = \frac{1}{\sqrt{6}}\Sigma^{*,0}, \quad T_{223} = \frac{1}{\sqrt{3}}\Sigma^{*,-},\\ &T_{133} = \frac{1}{\sqrt{3}}\Xi^{*,0}, \quad T_{233} = \frac{1}{\sqrt{3}}\Xi^{*,-}, \quad T_{333} = \Omega^-.\end{aligned} \tag{9}$$

The octet, decuplet, and octet-decuplet transition magnetic moment operators are needed in the one-loop calculation of nucleon magnetic form factors. The baryon octet magnetic Lagrangian is written as

$$\mathcal{L} = \frac{e}{4m_N}(\mu_D\mathrm{Tr}\bar{B}_v\sigma^{\mu\nu}\{F_{\mu\nu}^+, B_v\} + \mu_F\mathrm{Tr}\bar{B}_v\sigma^{\mu\nu}[F_{\mu\nu}^+, B_v]), \tag{10}$$

where

$$F_{\mu\nu}^+ = \frac{1}{2}(\zeta^\dagger F_{\mu\nu}Q\zeta + \zeta F_{\mu\nu}Q\zeta^\dagger). \tag{11}$$

Q is the charge matrix $Q = \mathrm{diag}\{2/3, -1/3, -1/3\}$. At the lowest order, the Lagrangian will generate the following nucleon magnetic moments:

$$\mu_p^{\mathrm{tree}} = \frac{1}{3}\mu_D + \mu_F, \qquad \mu_n^{\mathrm{tree}} = -\frac{2}{3}\mu_D. \tag{12}$$

The decuplet magnetic moment operator is expressed as

$$\mathcal{L} = -i\frac{e}{m_N}\mu_C q_{ijk}\bar{T}^{\mu}_{v,ikl}T^{\nu}_{v,jkl}F_{\mu\nu}, \tag{13}$$

where q_{ijk} and $q_{ijk}\mu_C$ are the charge and magnetic moment of the decuplet baryon T_{ijk}. The transition magnetic operator is

$$\mathcal{L} = i\frac{e}{2m_N}\mu_T F_{\mu\nu}(\epsilon_{ijk}Q^i_l\bar{B}^j_{vm}S^{\mu}_v T^{\nu,klm}_v + \epsilon^{ijk}Q^l_i\bar{T}^{\mu}_{v,klm}S^{\nu}_v B^m_{vj}). \tag{14}$$

In Ref. [45], the authors used μ_u, μ_d and μ_s instead of the μ_C and μ_T. For the particular choice, $\mu_s = \mu_d = -\frac{1}{2}\mu_u$, one finds the following relationship:

$$\mu_D = \frac{3}{2}\mu_u, \quad \mu_F = \frac{2}{3}\mu_D, \quad \mu_C = \mu_D, \quad \mu_T = -4\mu_D. \tag{15}$$

In our numerical calculations, the above formulas are used, and therefore all baryon magnetic moments are related to one parameter, μ_D.

In the heavy-baryon formalism, the propagators of the octet or decuplet baryon, j, are expressed as

$$\frac{i}{v\cdot k - \delta^{jN} + i\varepsilon} \quad \text{and} \quad \frac{iP^{\mu\nu}}{v\cdot k - \delta^{jN} + i\varepsilon}, \tag{16}$$

where $P^{\mu\nu}$ is $v^{\mu}v^{\nu} - g^{\mu\nu} - (4/3)S^{\mu}_v S^{\nu}_v$. $\delta^{ab} = m_b - m_a$ is the mass difference of between the two baryons. The propagator of meson j ($j = \pi$, K, η) is the usual free propagator, i.e.,

$$\frac{i}{k^2 - M_j^2 + i\varepsilon}. \tag{17}$$

III. NUCLEON MAGNETIC MOMENTS

In the heavy baryon formalism, the nucleon form factors are defined as

$$\langle B(p')|J_{\mu}|B(p)\rangle = \bar{u}(p')\left\{v_{\mu}G_E(Q^2) + \frac{i\epsilon_{\mu\nu\alpha\beta}v^{\alpha}S^{\beta}_v q^{\nu}}{m_N}G_M(Q^2)\right\}u(p), \tag{18}$$

where $q = p' - p$ and $Q^2 = -q^2$. According to the Lagrangian, the one-loop Feynman diagrams that contribute to the nucleon magnetic moments are plotted in Fig. 1. The intermediate baryons can be octets and decuplets.

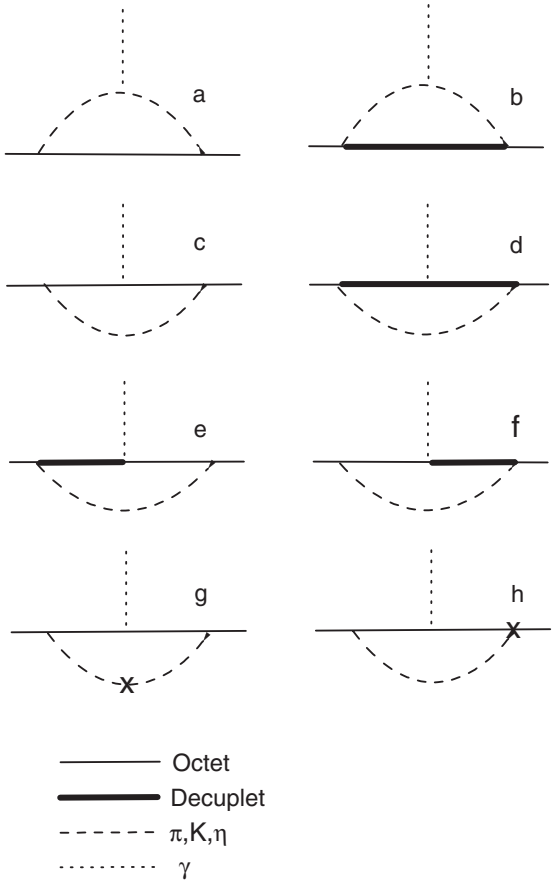

FIG. 1. Feynman diagrams for the nucleon magnetic moments. The last two diagrams, (g) and (h), only exist in the quenched case.

Diagrams (a) and (b) are for the leading order, while diagrams (c), (d), (e), and (f) enter at NLO. The last two diagrams exist only in the quenched case where the η' is degenerate with the pion and no K-meson loops contribute.

The loop contribution to nucleon magnetic form factors at leading order is expressed as

$$G_M^{p(\mathrm{LO})} = \frac{m_N}{8\pi^3 f_\pi^2}[\beta^{NN}_{1\pi(p)}I^{NN}_{1\pi} + \beta^{N\Lambda}_{1K(p)}I^{N\Lambda}_{1K} + \beta^{N\Sigma}_{1K(p)}I^{N\Sigma}_{1K} + \beta^{N\Delta}_{1\pi(p)}I^{N\Delta}_{1\pi} + \beta^{N\Sigma^*}_{1K(p)}I^{N\Sigma^*}_{1K}], \tag{19}$$

$$G_M^{n(\mathrm{LO})} = \frac{m_N}{8\pi^3 f_\pi^2}[\beta^{NN}_{1\pi(n)}I^{NN}_{1\pi} + \beta^{N\Sigma}_{1K(n)}I^{N\Sigma}_{1K} + \beta^{N\Delta}_{1\pi(n)}I^{N\Delta}_{1\pi} + \beta^{N\Sigma^*}_{1K(n)}I^{N\Sigma^*}_{1K}]. \tag{20}$$

The integration $I^{\alpha\beta}_{1j}$ is expressed as

$$I^{\alpha\beta}_{1j} = \int d^3k \frac{k_y^2 u(\vec{k}+\vec{q}/2)u(\vec{k}-\vec{q}/2)(\omega_j(\vec{k}+\vec{q}/2) + \omega_j(\vec{k}-\vec{q}/2) + \delta^{\alpha\beta})}{A^{\alpha\beta}_j}, \tag{21}$$

where

TABLE I. Coefficients β for the magnetic moments in the full QCD case.

	$\beta_{1\pi}^{NN}$	$\beta_{1K}^{N\Lambda}$	$\beta_{1K}^{N\Sigma}$	$\beta_{1\pi}^{N\Delta}$	$\beta_{1K}^{N\Sigma^*}$
Proton	$(D+F)^2$	$\frac{(D+3F)^2}{6}$	$\frac{(D-F)^2}{2}$	$\frac{2\mathcal{C}^2}{9}$	$-\frac{\mathcal{C}^2}{18}$
Neutron	$-(D+F)^2$	$\cdots$	$(D-F)^2$	$-\frac{2\mathcal{C}^2}{9}$	$-\frac{\mathcal{C}^2}{9}$
	$\beta_{2\pi}^{NN}$	$\beta_{2K}^{N\Lambda}$	$\beta_{2K}^{N\Sigma}$	$\beta_{2\pi}^{N\Delta}$	$\beta_{2K}^{N\Sigma^*}$
Proton	$\frac{(D+F)^2}{4}(\mu_D-\mu_F)$	$\frac{(D+3F)^2}{12}\mu_D$	$-\frac{(D-F)^2}{4}(\mu_D+2\mu_F)$	$\frac{40\mathcal{C}^2}{27}\mu_C$	$\frac{5\mathcal{C}^2}{27}\mu_C$
Neutron	$-\frac{(D+F)^2}{2}\mu_F$	$\frac{(D+3F)^2}{12}\mu_D$	$-\frac{(D-F)^2}{4}(\mu_D-2\mu_F)$	$-\frac{10\mathcal{C}^2}{27}\mu_C$	$-\frac{5\mathcal{C}^2}{27}\mu_C$
	$\beta_{2\eta}^{NN}$	$\beta_{3\pi}^{N\Delta}$	$\beta_{5K}^{N\Lambda\Sigma}$	$\beta_{5K}^{N\Sigma\Sigma^*}$	$\beta_{5K}^{N\Lambda\Sigma^*}$
Proton	$-\frac{(D-3F)^2}{12}(\mu_D+3\mu_F)$	$\frac{4(D+F)\mathcal{C}}{9}\mu_T$	$\frac{(D-F)(D+3F)}{6}$	$\frac{5(D-F)\mathcal{C}}{18}$	$\frac{(D+3F)\mathcal{C}}{18}$
Neutron	$-\frac{(D-3F)^2}{6}\mu_D$	$-\frac{4(D+F)\mathcal{C}}{9}\mu_T$	$-\frac{(D-F)(D+3F)}{6}$	$\frac{(D-F)\mathcal{C}}{18}$	$-\frac{(D+3F)\mathcal{C}}{18}$

$$A_j^{\alpha\beta} = \omega_j(\vec{k}+\vec{q}/2)\omega_j(\vec{k}-\vec{q}/2)(\omega_j(\vec{k}+\vec{q}/2)+\delta^{\alpha\beta}) \times(\omega_j(\vec{k}-\vec{q}/2)+\delta^{\alpha\beta})(\omega_j(\vec{k}+\vec{q}/2) + \omega_j(\vec{k}-\vec{q}/2)). \quad (22)$$

$\omega_j(\vec{k}) = \sqrt{m_j^2+\vec{k}^2}$ is the energy of the meson j. $\delta^{\alpha\beta}$ is the mass difference between baryon α and β. In our calculation, we use finite-range regularization with $u(\vec{k})$ the ultraviolet regulator. This leading-order contribution has been studied in the previous paper [12,15] which gives the leading analytic term to the magnetic moments. The first terms in Eqs. (19) and (20) come from the π meson cloud, while the last two terms correspond to the case where the intermediate baryons are decuplets.

The NLO contribution to the form factors is expressed as

$$G_M^{p(\mathrm{NLO})} = \frac{1}{48\pi^3 f_\pi^2}[\beta_{2\pi(p)}^{NN} I_{2\pi}^{NN} + \beta_{2K(p)}^{N\Sigma} I_{2K}^{N\Sigma} + \beta_{2K(p)}^{N\Lambda} I_{2K}^{N\Lambda} + \beta_{5K(p)}^{N\Lambda\Sigma} I_{5K}^{N\Lambda\Sigma} + \beta_{2\eta(p)}^{NN} I_{2\eta}^{NN} + \beta_{2\pi(p)}^{N\Delta} I_{2\pi}^{N\Delta} + \beta_{2K(p)}^{N\Sigma^*} I_{2K}^{N\Sigma^*} + \beta_{3\pi(p)}^{N\Delta} I_{3\pi}^{N\Delta} + \beta_{5K(p)}^{N\Sigma\Sigma^*} I_{5K}^{N\Sigma\Sigma^*} + \beta_{5K(p)}^{N\Lambda\Sigma^*} I_{5K}^{N\Lambda\Sigma^*}], \quad (23)$$

$$G_M^{n(\mathrm{NLO})} = \frac{1}{48\pi^3 f_\pi^2}[\beta_{2\pi(n)}^{NN} I_{2\pi}^{NN} + \beta_{2K(n)}^{N\Sigma} I_{2K}^{N\Sigma} + \beta_{2K(n)}^{N\Lambda} I_{2K}^{N\Lambda} + \beta_{5K(n)}^{N\Lambda\Sigma} I_{5K}^{N\Lambda\Sigma} + \beta_{2\eta(n)}^{NN} I_{2\eta}^{NN} + \beta_{2\pi(n)}^{N\Delta} I_{2\pi}^{N\Delta} + \beta_{2K(n)}^{N\Sigma^*} I_{2K}^{N\Sigma^*} + \beta_{3\pi(n)}^{N\Delta} I_{3\pi}^{N\Delta} + \beta_{5K(n)}^{N\Sigma\Sigma^*} I_{5K}^{N\Sigma\Sigma^*} + \beta_{5K(n)}^{N\Lambda\Sigma^*} I_{5K}^{N\Lambda\Sigma^*}], \quad (24)$$

where

$$I_{2j}^{\alpha\beta} = \int d^3k \frac{k^2 u^2(\vec{k})}{\omega_j(\vec{k})(\omega_j(\vec{k})+\delta^{\alpha\beta})^2}, \quad (25)$$

$$I_{5j}^{\alpha\beta\gamma} = \int d^3k \frac{k^2 u^2(\vec{k})}{\omega_j(\vec{k})(\omega_j(\vec{k})+\delta^{\alpha\beta})(\omega_j(\vec{k})+\delta^{\alpha\gamma}))}, \quad (26)$$

$$I_{3j}^{\alpha\beta} = \int d^3k \frac{k^2 u^2(\vec{k})}{\omega_j(\vec{k})^2(\omega_j(\vec{k})+\delta^{\alpha\beta})}. \quad (27)$$

All the coefficients β in front of the integrals are shown in Table I for full QCD. The coefficients of the leading-order contributions are functions of the coupling constants D, F, and $\mathcal{C}$. The coefficients of the NLO contribution are associated with the tree-level baryon magnetic moments.

The magnetic moment is defined as $\mu = G_M(Q^2=0)$. The total nucleon magnetic moments can be written as

$$\mu_p(m_\pi^2) = a_0^p + a_2^p m_\pi^2 + a_4^p m_\pi^4 + (Z-1)\mu_p^{\mathrm{tree}} + G_M^{p(\mathrm{LO})}(Q^2=0) + G_M^{p(\mathrm{NLO})}(Q^2=0), \quad (28)$$

$$\mu_n(m_\pi^2) = a_0^n + a_2^n m_\pi^2 + a_4^n m_\pi^4 + (Z-1)\mu_n^{\mathrm{tree}} + G_M^{n(\mathrm{LO})}(Q^2=0) + G_M^{n(\mathrm{NLO})}(Q^2=0), \quad (29)$$

where the wave function renormalization can be calculated as

$$Z = 1 - \frac{1}{48\pi^3 f_\pi^2}[\beta_\pi^{NN} I_{2j}^{NN} - \beta_\pi^{N\Delta} I_{2j}^{N\Delta} - \beta_K^{N\Lambda} I_{2j}^{N\Lambda} - \beta_K^{N\Sigma} I_{2j}^{N\Sigma} - \beta_K^{NN} I_{2j}^{N\Sigma^*} - \beta_\eta^{NN} I_{2j}^{NN}]. \quad (30)$$

The coefficients β in the wave function renormalization are listed in Table II.

With the exception of Figs. 1(a) and 1(b), the contributions of the diagrams in Fig. 1 are proportional to the tree-level moments, $\mu_{p(n)}^{\mathrm{tree}}$, expressed in Eq. (12). In the quenched case [10], the logarithmic divergence of the magnetic moment encountered in the chiral limit makes it necessary to replace the leading-order estimate $\mu_{p(n)}^{\mathrm{tree}}$ with the renormalized moment, effectively incorporating physics associated with higher-order terms of the expansion. To provide a connection between the quenched and full QCD expansions, we make this replacement for the full QCD case as well. Therefore, the expression for nucleon magnetic moments can be written as

TABLE II. Coefficients β and $\tilde{\beta}$ for the wave function renormalization in the full QCD and quenched cases.

Full QCD	β_π^{NN}	$\beta_\pi^{N\Delta}$	$\beta_K^{N\Lambda}$	$\beta_K^{N\Sigma}$	$\beta_K^{N\Sigma^*}$	β_η^{NN}
	$\frac{9}{4}(D+F)^2$	$2\mathcal{C}^2$	$\frac{1}{4}(3F+D)^2$	$\frac{15}{4}(D-F)^2$	$\frac{5}{6}\mathcal{C}^2$	$\frac{1}{2}(3F-D)^2$
Quenched	$\tilde{\beta}_\pi^{NN}$	$\tilde{\beta}_\pi^{N\Delta}$	$\tilde{\beta}_\eta^{NN}$	$\tilde{\beta}_{dh}^{NN}$	$\tilde{\beta}_h^{NN}$	
	$-\frac{9}{4}D^2-\frac{9}{4}F^2+\frac{15}{2}DF$	$\frac{1}{2}\mathcal{C}^2$	$-\frac{3}{2}D^2-\frac{3}{2}F^2+DF$	$\frac{3}{4}M_0^2(3F-D)^2$	$3(3F-D)(D-F)$	

$$\mu_{p(n)} = a_0^{p(n)} + a_2^{p(n)} m_\pi^2 + a_4^{p(n)} m_\pi^4 + \mu_{l1}^{p(n)} + (Z-1)\mu_{p(n)} + \frac{\mu_{l2}^{p(n)}}{\mu_{p(n)}^{\text{tree}}}\mu_{p(n)}, \tag{31}$$

where $\mu_{l1}^{p(n)}$ is the loop contribution from diagrams (a) and (b) in Fig. 1, while $\mu_{l2}^{p(n)}$ is the contribution from (c), (d), (e), and (f) expressed in the previous formulas. The above formula can be rewritten as

$$\mu_{p(n)} = \{a_0^{p(n)} + a_2^{p(n)} m_\pi^2 + a_4^{p(n)} m_\pi^4 + \mu_{l1}^{p(n)}\} \Big/ \left(2 - Z - \frac{\mu_{l2}^{p(n)}}{\mu_{p(n)}^{\text{tree}}}\right). \tag{32}$$

Since the lattice data of the magnetic moment are obtained in the quenched approximation, we should fit the lattice data using quenched chiral perturbation theory. In the quenched case, only the pion loop makes a contribution. The coefficients in the quenched case are shown in Table III. They can be obtained following the methodology of Ref. [19]. Remember, in this case, we have two more diagrams, i.e., (g) and (h) in Fig. 1.

The loop contribution to the nucleon magnetic moments at leading order in the quenched case is expressed as

$$\tilde{G}_M^{p(\text{LO})} = \frac{m_N}{8\pi^3 f_\pi^2}[\tilde{\beta}_{1\pi(p)}^{NN} I_{1\pi}^{NN} + \tilde{\beta}_{1\pi(p)}^{N\Delta} I_{1\pi}^{N\Delta} + \tilde{\beta}_{dh(p)}^{NN} I_{6\pi}^{NN}], \tag{33}$$

$$\tilde{G}_M^{n(\text{LO})} = \frac{m_N}{8\pi^3 f_\pi^2}[\tilde{\beta}_{1\pi(n)}^{NN} I_{1\pi}^{NN} + \tilde{\beta}_{1\pi(n)}^{N\Delta} I_{1\pi}^{N\Delta} + \tilde{\beta}_{dh(n)}^{NN} I_{6\pi}^{NN}], \tag{34}$$

where

$$I_{6j}^{NN} = \int d^3k \frac{k^2 u^2(\vec{k})}{\omega_j^5(\vec{k})}. \tag{35}$$

The NLO contribution can be written as

$$\tilde{G}_M^{p(\text{NLO})} = \frac{m_N}{48\pi^3 f_\pi^2}[\tilde{\beta}_{2\pi(p)}^{NN} I_{2\pi}^{NN} + \tilde{\beta}_{2\eta(p)}^{NN} I_{2\eta}^{NN} + \tilde{\beta}_{2\pi(p)}^{N\Delta} I_{2\pi}^{N\Delta} + \tilde{\beta}_{h(p)}^{NN} I_{2\pi}^{NN}], \tag{36}$$

$$\tilde{G}_M^{n(\text{NLO})} = \frac{m_N}{48\pi^3 f_\pi^2}[\tilde{\beta}_{2\pi(n)}^{NN} I_{2\pi}^{NN} + \tilde{\beta}_{2\eta(n)}^{NN} I_{2\eta}^{NN} + \tilde{\beta}_{2\pi(n)}^{N\Delta} I_{2\pi}^{N\Delta} + \tilde{\beta}_{h(n)}^{NN} I_{2\pi}^{NN}]. \tag{37}$$

In the quenched case, the wave function renormalization constant is obtained as $\tilde{Z}$:

$$\tilde{Z} = 1 - \frac{1}{48\pi^3 f_\pi^2}[\tilde{\beta}_\pi^{NN} I_{2j}^{NN} - \tilde{\beta}_\pi^{N\Delta} I_{2j}^{N\Delta} - \tilde{\beta}_{dh}^{NN} I_{6j}^{NN} - \tilde{\beta}_h^{NN} I_{2j}^{NN}], \tag{38}$$

where the coefficients $\tilde{\beta}$ are shown in Table II. For the double hairpin diagram, M_0 is the interaction strength.

Similar to the full QCD case, the quenched magnetic moments of the nucleon are expressed as

$$\tilde{\mu}_{p(n)} = \{a_0^{p(n)} + a_2^{p(n)} m_\pi^2 + a_4^{p(n)} m_\pi^4 + \tilde{\mu}_{l1}^{p(n)}\} \Big/ \left(2 - \tilde{Z} - \frac{\tilde{\mu}_{l2}^{p(n)}}{\tilde{\mu}_{p(n)}^{\text{tree}}}\right), \tag{39}$$

where $\tilde{\mu}_{l1}^{p(n)}$ is the loop contribution from diagrams (a) and (b) in Fig. 1 with quenched coefficients, while $\tilde{\mu}_{l2}^{p(n)}$ is the contribution from the other diagrams. Because the simulation is on a lattice with length L in the spatial dimensions, the momentum integral is replaced by a discrete sum over the momentum, i.e.,

TABLE III. Coefficients $\tilde{\beta}$ for the magnetic moments in the quenched case.

	$\tilde{\beta}_{1\pi}^{NN}$	$\tilde{\beta}_{1\pi}^{N\Delta}$	$\tilde{\beta}_{dh}^{NN}$	
Proton	$\frac{4}{3}D^2$	$\frac{\mathcal{C}^2}{6}$	$-\frac{(3F-D)^2}{72m_N}M_0^2(\mu_D+3\mu_F)$	
Neutron	$-\frac{4}{3}D^2$	$-\frac{\mathcal{C}^2}{6}$	$\frac{(3F-D)^2}{36m_N}M_0^2\mu_D$	
	$\tilde{\beta}_{2\pi}^{NN}$	$\tilde{\beta}_{2\eta}^{NN}$	$\tilde{\beta}_{2\pi}^{N\Delta}$	$\tilde{\beta}_h^{NN}$
Proton	$(\frac{31}{36}D^2-\frac{1}{4}F^2-\frac{1}{2}DF)\mu_D$	$\frac{3D^2+3F^2-2DF}{12}(\mu_D+3\mu_F)$	$\frac{5}{9}\mathcal{C}^2\mu_C$	$\frac{(3F-D)(F-D)}{3}(\mu_D+3\mu_F)$
Neutron	$-(\frac{11}{18}D^2-\frac{1}{2}F^2-\frac{19}{15}DF)\mu_D$	$\frac{-3D^2-3F^2+2DF}{2}\mu_D$	$-\frac{5\mathcal{C}^2}{18}\mu_C$	$\frac{2(3F-D)(D-F)}{3}\mu_D$

$$\int d^3k \Rightarrow \left(\frac{2\pi}{aL}\right)^3 \sum_{k_x,k_y,k_z}, \tag{40}$$

where the momenta k_x, k_y, and k_z are given by $2\pi n/L$ and the infinite sum is regulated by the finite-range regulator. By fitting the quenched lattice data with Eq. (39), one can get the parameters a_i. The full QCD results are then obtained with Eq. (32). In all the above formulas, the nucleon mass is chosen to be physical mass, m_N, and does not change with the pion mass. This is because the lattice data we will extrapolate are multiplied by the ratio m_N/m_N', where m_N' is the pion-mass-dependent nucleon mass [46]. In this way, the magnetic moments are presented in terms of a constant unit, i.e., the nuclear magneton.

IV. NUMERICAL RESULTS

In the numerical calculations, the parameters are chosen as $D = 0.76$ and $F = 0.50$ ($g_A = D + F = 1.26$). The coupling constant $\mathcal{C}$ is chosen to be -1.2 which is the same as Ref. [47]. The regulator, $u(k)$, may be chosen as a monopole, dipole, or Gaussian function, since all have been shown to yield similar results [48]. In our calculations, the dipole function is used:

$$u(k) = \frac{1}{(1 + k^2/\Lambda^2)^2}, \tag{41}$$

with $\Lambda = 0.8$ GeV.

The K- and η-meson masses have relationships with the pion mass according to

$$m_K^2 = \frac{1}{2}m_\pi^2 + m_K^2|_{\text{phy}} - \frac{1}{2}m_\pi^2|_{\text{phy}}, \tag{42}$$

$$m_\eta^2 = \frac{1}{3}m_\pi^2 + m_\eta^2|_{\text{phy}} - \frac{1}{3}m_\pi^2|_{\text{phy}} \tag{43}$$

and enable a direct relationship between the meson dressings of the nucleon magnetic moments and the pion mass.

We begin by considering nucleon magnetic moments from the CSSM Lattice Collaboration [46]. The leading-order result of the proton magnetic moment versus m_π^2 is shown in Fig. 2. The solid line is for the finite-volume quenched-QCD fit and the dashed, dotted, and dashed-dotted lines are for the infinite-volume full QCD results of tree level, leading loop, and sum of tree level and leading loop, respectively. One can see that quenched lattice results can be described very well in quenched chiral effective field theory. At the physical pion mass, the proton magnetic moment $\tilde{\mu}_p$ is about 2.25 which is significantly smaller than the experimental data. With the obtained fitting parameters a_i, the full QCD results are determined and illustrated in the figure.

In the quenched case, the loop contribution is small. While quenched-QCD coefficients of nonanalytic terms are typically smaller than in the full QCD case, the dominant effect here is that the momentum integration is replaced by the finite-volume sum. The loop contribution in full QCD gives the dominant curvature of the pion-mass dependence of the proton magnetic moment. The proton magnetic moment in the full QCD case is significantly larger. At the physical pion mass, the proton magnetic moment in the full QCD case, μ_p, is approximately $2.95\mu_N$ which is comparable with the experimental value, $2.79\mu_N$.

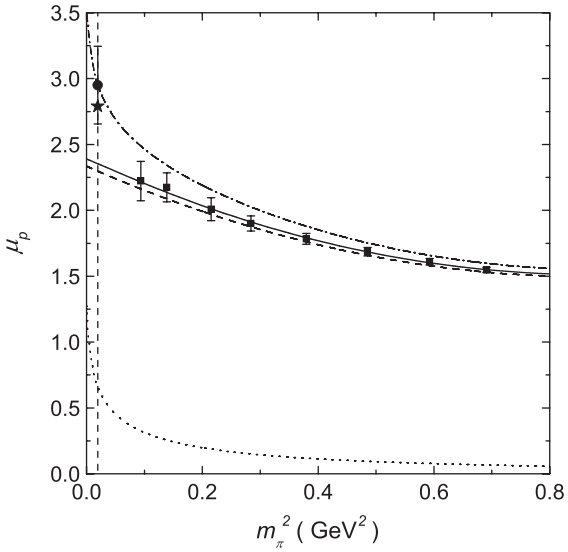

FIG. 2. The proton magnetic moment as a function of the squared pion mass. The solid line illustrates the finite-volume quenched-QCD fit to the lattice results. The dashed, dotted, and dashed-dotted lines correspond to the infinite-volume full-QCD results at tree level, leading loop, and sum of tree level and leading loop, respectively.

In the FRR, except for the fitting parameters a_i, there is only one free parameter, Λ, which is set to be 0.8 GeV. If we vary Λ from 0.6 to 1 GeV, the leading-order proton magnetic moment in full QCD will change by about 8% from the central value. At NLO, though both the wave function renormalization and loop contribution also depend on Λ, the final result is less sensitive to it. Therefore, as an estimate, we added the error bar (10% of its central value) to the extrapolated value at physical pion mass in each figure. The empirical value of the nucleon magnetic moment is also plotted in each figure with a solid star.

The leading-order result for the neutron magnetic moment versus m_π^2 is shown in Fig. 3. Again, the finite-volume quenched-QCD lattice results are described very well by finite-volume finite-range regularized quenched chiral effective field theory. The curvature of the line is small. At the physical pion mass, the finite-volume quenched neutron magnetic moment is around -1.5. The associated full QCD results of tree level, leading loop, and sum of tree level and leading loop are shown as well. Similar to the proton case, the loop contribution changes

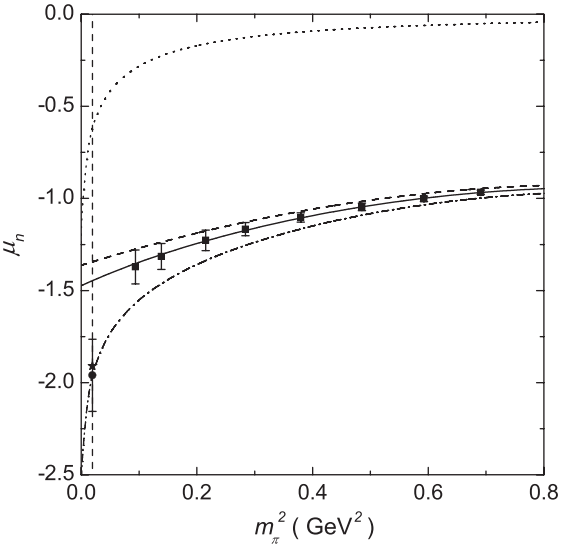

FIG. 3. The neutron magnetic moment as a function of the squared pion mass. The solid line illustrates the finite-volume quenched-QCD fit. The dashed, dotted, and dashed-dotted lines correspond to the infinite-volume full-QCD results of tree level, leading loop, and sum of tree level and leading loop contribution, respectively.

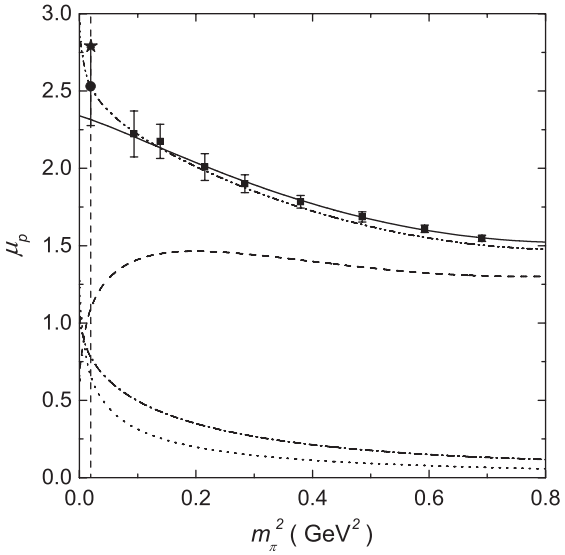

FIG. 4. The proton magnetic moment versus squared pion mass. The solid line illustrates the finite-volume quenched-QCD fit. The dashed, dotted, dashed-dotted, and dashed-dot-dotted lines correspond to the infinite-volume full-QCD results of tree level, leading loop, NLO loop, and sum of tree level and loop contribution, respectively.

smoothly at large pion mass and drops quickly at small pion masses. The total value of neutron magnetic moment from our leading-order calculations is $\mu_n \simeq -1.96\mu_N$, similar to the physical value of $-1.91\mu_N$.

The NLO result for the proton magnetic moment versus m_π^2 is shown in Fig. 4. The solid line is the finite-volume quenched-QCD result. The dashed, dotted, dashed-dotted, and dashed-dot-dotted lines are for the infinite-volume full-QCD results of tree level, leading order loop, NLO loop, and sum of tree and loop contribution, respectively. At NLO, the quenched lattice results continue to be described well by finite-volume quenched chiral effective field theory. However, at NLO, the approach to the chiral limit displays some downward curvature associated with the new wave function renormalization contributions which appear only at NLO. The wave function renormalization constant Z decreases quickly at small pion mass.

At the physical pion mass, the infinite-volume tree-level contribution to the proton magnetic moment changes from 2.30 to 1.10. The leading loop contribution at the physical pion mass is 0.65. The NLO loop contribution has a smaller curvature than the leading loop. It contributes 0.78 to the proton magnetic moment. The sum of tree level, leading loop, and NLO loop contribution to the proton magnetic moment is $2.53\mu_N$ to be compared with the experimental value of $2.79\mu_N$.

The NLO result for neutron magnetic moment μ_n versus m_π^2 is shown in Fig. 5. The meaning of the different types of lines are the same as for Fig. 4. Here, the wave function renormalization has a more subtle effect. As anticipated, the NLO loop contribution has a smaller curvature than the leading-order loop contribution. At the physical pion mass, the tree level, leading loop, and NLO loop contribute to the neutron magnetic moment -0.52, -0.62 and $-0.66\mu_N$, respectively. The total neutron magnetic moment at NLO is $-1.80\mu_N$ which remains close to the experimental value of $-1.91\mu_N$.

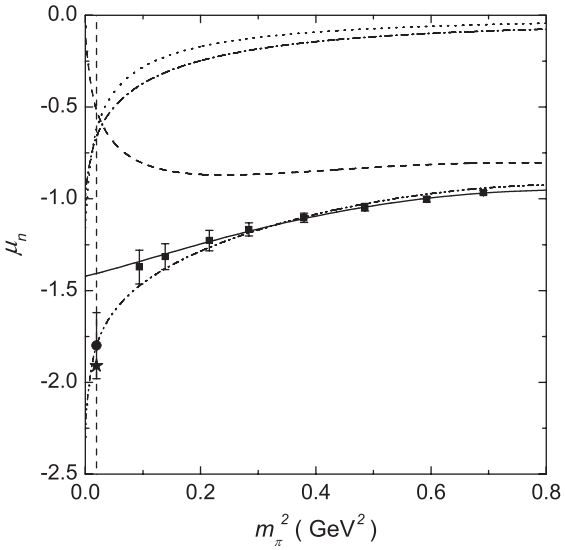

FIG. 5. The neutron magnetic moment versus squared pion mass. The solid line illustrates the quenched-QCD fit. The dashed, dotted, dashed-dotted, and dashed-dot-dotted lines correspond to the infinite-volume full-QCD results of tree level, leading loop, NLO loop, and sum of tree level and loop contribution, respectively.

We should mention that when we calculate the NLO loop contribution, the tadpole diagram is not included explicitly. That is, the tadpole contribution is handled by adjusting the parameters a_i' to a_i, so that

$$a_0' + a_2' m_\pi^2 + a_4' m_\pi^4 + \mu_{tad} \simeq a_0 + a_2 m_\pi^2 + a_4 m_\pi^4, \quad (44)$$

where $\mu_{\rm tad}$ is the tadpole contribution to the magnetic moments. In Ref. [11], the chiral extrapolation did explicitly include this tadpole diagram, but the numerical results were almost the same if we refit the lattice data without this diagram. This means that, in practice, the new parameters, a_i, can compensate the contribution of the tadpole diagram. In the present work, we explored both the explicit and implicit inclusion of the tadpole term, with the numerical results clearly favoring the approximation where the fitting parameters on the right-hand side of Eq. (44) are the same in the quenched and full QCD cases.

Chiral symmetry can be realized in a number of ways, resulting in different forms for the effective Lagrangian. In Ref. [49], the authors applied two different Lagrangian densities incorporating chiral symmetry to the problem of pion-nucleon scattering, with the nucleon represented by an MIT bag. In one case, the interaction was confined to the bag surface, where only a Yukawa type $NN\pi$ interaction appeared. The other formulation involved a volume interaction, where a contact term (four-particle $NN\pi\pi$ term) is required. Their conclusion was that transforming from the surface interaction to the volume interaction amounts to summing the contribution from all excited intermediate states of the confined quarks. That is, the two formulations give equivalent results if excited intermediate states are included. One can also study the magnetic moments with the pseudoscalar nucleon-meson interaction where no tadpole diagram appears—c.f. Refs. [2–4]. With this background, we conclude that the tadpole contribution to the magnetic moments from the contact term corresponds to the contribution of diagram (c) in Fig. 1 summed over an infinite set of highly excited baryon states, and phenomenologically this appears to be appropriately incorporated through Eq. (44).

V. SUMMARY

We have extrapolated quenched lattice QCD results for nucleon magnetic moments extending into the chiral regime [46] to the physical pion mass using finite-volume finite-range regularized chiral effective field theory. Here, the NLO contributions are included, with the numerical results showing that the quenched lattice results are described very well. By fitting quenched lattice data, the parameters a_i can be obtained, and, using the dipole regulator parameter of 0.8 GeV, the full QCD results are predicted. The infinite-volume full QCD results obtained at the physical pion mass are in reasonable agreement with experiment at both leading order and NLO. Thus, finite-range regularized chiral effective field theory provides an effective formalism for describing physical quantities at large pion mass and connecting quenched QCD and full QCD in a quantitative manner. This formalism leads to a remarkably reliable, albeit model-dependent, way of resumming terms in the chiral expansion. The parameters and results are summarized in Table IV.

TABLE IV. The obtained coefficients a_i and magnetic moments.

	a_0	a_2	a_4	$\tilde{\mu}^{\rm LO}$	$\tilde{\mu}^{\rm NLO}$	$\mu^{\rm LO}$	$\mu^{\rm NLO}$	Exp.
Proton	2.34	−2.08	1.24	2.35	2.31	2.95	2.53	2.79
Neutron	−1.39	1.17	−0.70	−1.45	−1.41	−1.96	−1.80	−1.91

It is interesting how the NLO contributions come in a compensating fashion. While each NLO contribution displays significant curvature in the chiral regime, the net contribution is relatively smooth and otherwise easily compensated for by the residual series expansion. We expect that this qualitative behavior will continue as additional higher-order terms are introduced, as we are informed by the lattice QCD results displaying a smooth slowly varying quark mass dependence. Indeed, it will be interesting to examine more physical quantities to gain a deeper understanding of the utility of finite-range regularized chiral effective field theory.

ACKNOWLEDGMENTS

This work is supported in part by DFG and NSFC (CRC 110), by the National Natural Science Foundation of China (Grant No. 11035006), and by the Australian Research Council through Grants No. FL0992247 (AWT) and No. DP110101265 (DBL and RDY), and through the ARC Centre of Excellence for Particle Physics at the Terascale.

[1] A. W. Thomas, Nucl. Phys. B, Proc. Suppl. **119**, 50 (2003).
[2] D. H. Lu, A. W. Thomas, and A. G. Williams, Phys. Rev. C **57**, 2628 (1998).
[3] V. E. Lyubovitskij, P. Wang, T. Gutsche, and A. Faessler, Phys. Rev. C **66**, 055204 (2002).
[4] A. Faessler, T. Gutsche, M. A. Ivanov, V. E. Lyubovitskij, and P. Wang, Phys. Rev. D **68**, 014011 (2003).
[5] D. B. Leinweber, D. H. Lu, and A. W. Thomas, Phys. Rev. D **60**, 034014 (1999).

[6] D. B. Leinweber, A. W. Thomas, K. Tsushima, and S. V. Wright, Phys. Rev. D **61**, 074502 (2000).
[7] D. B. Leinweber, A. W. Thomas, and R. D. Young, Phys. Rev. Lett. **92**, 242002 (2004).
[8] C. R. Allton, W. Armour, D. B. Leinweber, A. W. Thomas, and R. D. Young, Phys. Lett. B **628**, 125 (2005).
[9] W. Armour, C. R. Allton, D. B. Leinweber, A. W. Thomas, and R. D. Young, J. Phys. G **32**, 971 (2006).
[10] R. D. Young, D. B. Leinweber, and A. W. Thomas, Phys. Rev. D **71**, 014001 (2005).
[11] P. Wang, A. W. Thomas, D. B. Leinweber, and R. D. Young, Phys. Rev. D **75**, 073012 (2007).
[12] D. B. Leinweber, S. Boinepalli, I. Cloet, A. Thomas, A. Williams, R. Young,J. Zanotti, and J. Zhang, Phys. Rev. Lett. **94**, 212001 (2005).
[13] D. B. Leinweber, S. Boinepalli, A. Thomas, P. Wang, A. Williams, R. Young, J. Zanotti, and J. Zhang, Phys. Rev. Lett. **97**, 022001 (2006).
[14] P. Wang, A. W. Thomas, D. B. Leinweber, and R. D. Young, Phys. Rev. D **79**, 094001 (2009).
[15] P. Wang, A. W. Thomas, D. B. Leinweber, and R. D. Young, Phys. Rev. C **79**, 065202 (2009).
[16] P. Wang and A. W. Thomas, Phys. Rev. D **81**, 114015 (2010).
[17] J. N. Labrenz and S. R. Sharpe, Phys. Rev. D **54**, 4595 (1996).
[18] M. J. Savage, Nucl. Phys. **A700**, 359 (2002).
[19] D. B. Leinweber, Phys. Rev. D **69**, 014005 (2004).
[20] D. Arndt and B. C. Tiburzi, Phys. Rev. D **68**, 094501 (2003).
[21] B. C. Tiburzi, Phys. Rev. D **71**, 054504 (2005).
[22] R. D. Young, D. B. Leinweber, A. W. Thomas, and S. V. Wright, Phys. Rev. D **66**, 094507 (2002).
[23] S. Sasaki, K. Orginos, S. Ohta, and T. Blum, Phys. Rev. D **68**, 054509 (2003).
[24] R. G. Edwards, G. Fleming, P. Hägler, J. Negele, K. Orginos, A. Pochinsky, D. Renner, D. Richards, and W. Schroers, Phys. Rev. Lett. **96**, 052001 (2006).
[25] T. Yamazaki, Y. Aoki, T. Blum, H. Lin, M. Lin, S. Ohta, S. Sasaki, R. Tweedie, and J. Zanotti, Phys. Rev. Lett. **100**, 171602 (2008).
[26] S. Capitani,M. D. Morte, G. von Hippel, B. Jäger, A. Jüttner, B. Knippschild, H. B. Meyer, and H. Wittig, Phys. Rev. D **86**, 074502 (2012).
[27] S. Aoki *et al.*, Phys. Rev. D **62**, 094501 (2000).
[28] S. N. Syritsyn *et al.*, Phys. Rev. D **81**, 034507 (2010).
[29] S. Sasaki and T. Yamazaki, Phys. Rev. D **78**, 014510 (2008).
[30] C. Alexandrou, G. Koutsou, J. W. Negele, and A. Tsapalis, Phys. Rev. D **74**, 034508 (2006).
[31] H. H. Matevosyan, G. A. Miller, and A. W. Thomas, Phys. Rev. C **71**, 055204 (2005).
[32] M. Goeckeler, T. Hemmert, R. Horsley, D. Pleiter, P. Rakow, A. Schäfer, and G. Schierholz, Phys. Rev. D **71**, 034508 (2005).
[33] W. Wilcox, T. Draper, and K. F. Liu, Phys. Rev. D **46**, 1109 (1992).
[34] J. M. M. Hall, D. B. Leinweber, and R. D. Young, Phys. Rev. D **85**, 094502 (2012).
[35] J. D. Ashley, D. B. Leinweber, A. W. Thomas, and R. D. Young, Eur. Phys. J. A **19**, 9 (2004).
[36] S. Boinepalli, D. Leinweber, P. Moran, A. Williams, J. Zanotti, and J. Zhang, Phys. Rev. D **80**, 054505 (2009).
[37] S. Collins *et al.*, Phys. Rev. D **84**, 074507 (2011).
[38] T. Yamazaki, Y. Aoki, T. Blum, H.-W. Lin, S. Ohta, S. Sasaki, R. Tweedie, and J. Zanotti, Phys. Rev. D **79**, 114505 (2009).
[39] K. Goeke, J. Grabis, J. Ossmann, P. Schweitzer, A. Silva, and D. Urbano, Phys. Rev. C **75**, 055207 (2007).
[40] M. Gockeler *et al.*, Proc. Sci., LAT2007 (2007) 161.
[41] F. K. Guo, C. Hanhart, F. J. Llanes-Estrada, and U.-G. Meissner, Phys. Lett. B **678**, 90 (2009).
[42] E. E. Jenkins and A. V. Manohar, Phys. Lett. B **255**, 558 (1991).
[43] V. Bernard, N. Kaiser, J. Kambor, and U. G. Meissner, Nucl. Phys. **B388**, 315 (1992).
[44] V. Bernard, Prog. Part. Nucl. Phys. **60**, 82 (2008).
[45] P. Ha and L. Durand, Phys. Rev. D **58**, 093008 (1998); **67**, 073017 (2003).
[46] S. Boinepalli, D. B. Leinweber, A. G. Williams, J. M. Zanotti, and J. B. Zhang, Phys. Rev. D **74**, 093005 (2006).
[47] E. Jenkins, M. Luke, A. V. Manohar, and M. J. Savage, Phys. Lett. B **302**, 482 (1993); **388**, 866(E) (1996).
[48] R. D. Young, D. B. Leinweber, and A. W. Thomas, Prog. Nucl. Phys. **50**, 399 (2003).
[49] B. K. Jennings and O. V. Maxwell, Nucl. Phys. **A422**, 589 (1984).